E 28) E 281

PUB-78-104-E
E-0002
E-0281

ρ^0 Production in π^-p Interactions at 100, 200, and 360 GeV/c

P.D. Higgins, W.D. Shephard, N.N. Biswas, J.M. Bishop, R.L. Bolduc, N.M. Cason, and R.C. Ruchti
Department of Physics
University of Notre Dame, Notre Dame, Indiana 46556

W.D. Walker, J.S. Loos[a], L.R. Fortney, A.T. Goshaw and W.J. Robertson
Department of Physics
Duke University, Durham, North Carolina 27706

L. Voyvodic and R.J. Walker
Fermi National Accelerator Laboratory
Batavia, Illinois 60510

E.W. Anderson, H.B. Crawley, A. Firestone, J.S. Hendrickson, W.J. Kernan, J.W. Lamsa, and D.L. Parker
Department of Physics
Iowa State University, Ames, Iowa 50010

G.A. Snow
Department of Physics and Astronomy
University of Maryland, College Park, Maryland 20742

B.Y. Oh, M. Pratap, G. Sionakides, G.A. Smith, and J. Whitmore
Department of Physics
Michigan State University, East Lansing, Michigan 48824

V. Sreedhar[b], G. Levman[a], B.M. Schwarzschild, and T.S. Yoon
Department of Physics
University of Toronto, Toronto, Ontario M5S 1A7, Canada

G. Hartner[c] and P.M. Patel
Department of Physics
McGill University, Montreal, Quebec H3C 3G7, Canada

Abstract

Inclusive and semi-inclusive cross sections for ρ^0 production in 100, 200 and 360 GeV/c π^-p interactions are presented. Differential cross sections for ρ^0 production as functions of c.m. rapidity and transverse momentum are compared with the corresponding differential cross sections for pion production. Effects of various methods of estimating background on the values obtained for ρ^0 production cross sections are discussed. About 10% of the final-state charged pions appear to come from ρ^0 decay. Thus, while ρ^0 production and decay is a significant source of final-state pions, other sources must contribute the majority of the produced pions.

I. Introduction

The contribution of resonance production to inclusive particle production in strong interactions is currently a subject of great interest. If resonances are the source of a significant fraction of the observed pion production, they must be considered a factor in producing the short-range two-particle correlations found at high energies. Vector meson production and decay may also be a source of much of the lepton production observed in hadronic reactions. Detailed studies of resonance production at the highest available energies are necessary for our understanding of these effects.

In this paper we consider the energy dependence of $\rho^0(770)$ production in π^-p interactions. In particular we concentrate on data from 100, 200, and 360 GeV/c π^-p experiments performed in the Fermilab hybrid spectrometer consisting of the 30-inch bubble chamber together with downstream wide-gap optical spark chambers and upstream proportional wire chambers. Specifically,

we study inclusive and semi-inclusive production in the reactions

$$\pi^- p \to \rho^0 + \text{anything}, \qquad (1)$$

In Section II the data samples are discussed briefly. In Section III we determine the inclusive and semi-inclusive cross sections for reaction (1) and consider the energy dependance of the inclusive ρ^0 cross sections and the dependence of the semi-inclusive ρ^0 cross sections on energy and charge multiplicity. In Section IV we compare reaction (1) with

$$\pi^- p \to \pi^* + \text{anything}. \qquad (2)$$

In particular we study the energy dependence of $\langle \rho^0 \rangle$, the average number of rho's produced per event, and the ratio of ρ^0 production to π production. We also compare the transverse momentum spectrum for ρ^0 mesons to that for π^+ mesons. In Section V we examine the energy dependence of ρ^0 production in various ranges of center of mass (c.m.) rapidity y^* of the ρ^0, and compare the overall rapidity distributions for reactions (1) and (2). In Section VI we summarize our results. In Appendix A we discuss alternative methods of estimating background distributions for use in determining ρ^0 production cross sections.

II. Experimental Details

The data used in the following analysis were obtained in experiments utilizing the Fermilab 30-inch hydrogen bubble chamber-wide gap spark chamber hybrid spectrometer. The bubble chamber served as a vertex detector and provided accurate measurements for low-momentum tracks. The downstream wide-gap optical spark chambers were used in conjunction with the bubble chamber to provide improved momentum resolution for fast forward tracks.

Momentum measurements from the hybrid system have been used whenever they are available. Upstream proportional wire chambers were used to determine the direction and position of the beam particle for each event. Protons with laboratory momenta less than 1.4 GeV/c have been identified on the basis of bubble density. All other charged particles without visible decays have been assumed to be pions. Further details of the experiments have been presented elsewhere[1].

Our data samples consist of approximately 30,000 events at 360 GeV/c, 17,000 events at 200 GeV/c, and 7,700 events at 100 GeV/c. In determining mass distributions and cross sections, the events of each multiplicity are weighted so that the semi-inclusive topological cross sections correspond to the published values[2].

III. Inclusive and Semi-Inclusive ρ^0 Production Cross Sections

A. Determination of Cross Sections

A major problem in determining cross sections for ρ^0 production at high energies is the large combinatorial background which dominates multiparticle effective-mass distributions. Typically the signal-to-noise ratio in the ρ^0 mass region in $\pi^+\pi^-$ mass distributions is only a few percent at Fermilab energies. This can be seen in Fig. 1 where we show the inclusive $\pi^+\pi^-$ mass spectra for each of our three energies. In each case a shoulder is observed above a smooth background in the vicinity of the ρ^0 mass. It is clear that cross section estimates for ρ^0 production can be significantly influenced by the parametrization used for the background. In order to obtain results which are directly comparable to published results at other energies, we have used fitting techniques similar to those previously used[3-6] at lower energies.

It has been observed[4,6] that to first approximation the background under the ρ^0 mass region falls exponentially with increasing mass. Thus, if the mass spectrum is multiplied by an appropriate exponential in mass the strong variation of background (phase space) is removed and the resonance contributions may be more clearly observed. Depending on the range of mass fitted and the statistical accuracy of the data it is often necessary to use exponential terms of higher order in mass to obtain good fits to the data. We find that over the mass range $0.56 < M(\pi^+\pi^-) < 1.5$ GeV the backgrounds in our samples can be well described by functions of the form $A \exp(BM + CM^2)$ where the constants A, B and C may vary for different samples. In determining ρ^0 production cross sections we have assumed that the effective phase space for resonance production has the same mass dependence as this background.

We have fitted the inclusive mass distributions in the range 0.56 - 1.50 GeV with a function of the form

$$\frac{d\sigma}{dM} = A \exp(BM + CM^2) + D \cdot BW \cdot \exp(BM + CM^2) \qquad (3)$$

where A, B, C and D are constants to be determined and BW is a P-wave Breit-Wigner function

$$BW = \frac{MM_o\Gamma}{(M^2 - M_o^2)^2 + M_o^2\Gamma^2} \qquad (4)$$

where M_o and Γ are the mass and width of the resonance. For a P-wave resonance we use $\Gamma = \Gamma_o(k/k_o)^3$ where k is the pion momentum in the dipion rest frame and $k = k_o$ at the resonance mass $M = M_o$. After studying the effects of varying M_o and Γ_o we have fixed them at the values $M_o = 0.760$ GeV and

$\Gamma_o = 0.160$ GeV for the final fits. This estimate for Γ_o is consistent with adding an average $\pi^+\pi^-$ mass resolution of 0.050 GeV in quadrature with (0.152 ± 0.003) GeV, the nominal ρ^0 width[7]. Studies of the resolution[8] in $\pi^+\pi^-$ effective mass show this choice to be reasonable at all three incident energies. The resulting fits and background distributions are shown in Fig. 1. The inclusive ρ^0 production cross sections are given in Table I.

Proceeding in a similar fashion we have fitted the semi-inclusive $M(\pi^+\pi^-)$ distribution for each charge multiplicity n with the form (3). The resulting semi-inclusive ρ^0 production cross sections are given in Table I which also lists the sum of the semi-inclusive cross sections as well as other determinations of the inclusive cross section. Errors quoted in Table I include some allowance for the observed effects of small variations of the mass range and resonance parameters on the fitted cross sections. All fits gave acceptable χ^2 values. At each energy the agreement between the sum of the semi-inclusive cross sections and the inclusive cross section is quite satisfactory. In Fig. 2 are shown the semi-inclusive mass distributions at each energy for n = 6, 8, 10, 12 together with the results of the fits. The background contributions are shown as dashed lines in the resonance region.

In order to determine the effects of our assumptions about the shape of the background on our cross section values, we have tried other parametrizations including a simple exponential function and a variety of polynomial forms. In general the resulting ρ^0 cross sections were consistent within errors with those quoted in Table I whenever acceptable fits were obtained.

While the average resolution in $M(\pi^+\pi^-)$ at the ρ^0 mass is about 50

MeV, the resolution varies greatly with the longitudinal momentum of the $\pi^+\pi^-$ pair. This variation increases with increasing incident momentum. The calculated variation is sufficiently small over the entire kinematic range at 100 and 200 GeV/c that use of a constant $\Gamma_o = 0.160$ GeV in the fitting does not cause difficulties. At 360 GeV/c, however, the average $M(\pi^+\pi^-)$ resolution at the ρ^o mass is about 0.220 GeV for $\pi^+\pi^-$ pairs having c.m. rapidities in the range $+1 < y^* < +3$. Thus we have investigated the possibility that in performing a single fit to the whole sample we are underestimating the ρ^o cross section. We have fitted the distributions for various regions of y^* using different values of Γ_o consistent with the calculated resolution. Results are discussed in more detail in Section V. The total cross sections thus obtained are also shown in Table I and agree within statistics with the other determinations. We have also performed fits to samples consisting only of events in which momentum information utilizing the complete hybrid system is available for one or more tracks. The momentum resolution in the sample is considerably improved. Resulting estimates of fast-forward ρ^o production are consistent with those obtained using the whole sample and an increased value for Γ_o.

As our best estimates of the inclusive ρ^o cross section we use weighted averages of the three values obtained by the different methods described above. The resulting values are 7.65 ± 0.46, 8.54 ± 0.41, and 8.55 ± 0.17 mb, at 100, 200, and 360 GeV/c, respectively.

A recent publication[9] from the Split Field Magnet group at the ISR describes a completely different method of estimating the background in the $M(\pi^+\pi^-)$ distribution and of determining resonance cross sections. Their studies of neutral

vector meson production in pp collisions at c.m. energy $\sqrt{s} = 53$ GeV yield values for the number of resonances per event considerably larger than the corresponding numbers commonly obtained in analyses such as we have used at lower energies. Jancso et al.[9] determine background curves for their two-particle effective mass distributions by combining randomly selected tracks from different events. We find that background distributions obtained in this manner do not provide good representations of our data. However, for comparison and completeness we present results from a study of such backgrounds in Appendix A.

B. Variation of Inclusive Cross Section with Incident Energy

We have collected available data[3-6, 10-16] on inclusive ρ^o production in π^*p and pp interactions. In Fig. 3 are plotted the data[17] on inclusive ρ^o production cross sections as a function of s, the square of the total c.m. energy. We observe that for both π^*p and pp interactions the cross section appears to rise linearly with $\ell n\, s$, although the rise is more rapid in the pp case. If we separately fit the π^*p and pp data with a form $\sigma(\rho^o) = A + B\, \ell n\, s$ we obtain: for π^*p, $\sigma(\rho^o)$ (mb) = (-0.24 ± 0.10) + (1.38 ± 0.04) $\ell n\, s$ with χ^2/DF = 1.27, and for pp $\sigma(\rho^o)$ (mb) = (-9.18 ± 1.66) + (3.31 ± 0.50) $\ell n\, s$ with χ^2/DF = 0.08. These results are qualitatively similar to those previously presented by Bartke et al.[5], by Chliapnikov[18], and more recently by Wroblewski[19]. If, however, we fit only the four π^-p data points above $s = 100$ GeV^2, we obtain a best fit (dashed curve) consistent with a slower increase in $\sigma(\rho^o)$ at large s: $\sigma(\rho^o)$ (mb) = (4.59 ± 0.13) + (0.61 ± 0.02) $\ell n\, s$ with $\chi^2/DF = 0.53$.

Another commonly used form in which to present the data is to plot $\langle \rho^o \rangle$, the mean number of ρ^o mesons per inelastic interaction, as a function of s. These data are shown in Fig. 4. Best fits to the form $\langle \rho^o \rangle = C + D \ln s$ are $\langle \rho^o \rangle = (0.03 \pm 0.01) + (0.057 \pm 0.002) \ln s$ with $\chi^2/DF = 1.10$ for all $\pi^* p$ data and $\langle \rho^o \rangle = (-0.23 \pm 0.06) + (0.09 \pm 0.02) \ln s$ for pp data. Again, the $\pi^- p$ data above $s = 100$ GeV^2 are consistent with a less rapid rise: $\langle \rho^o \rangle = (0.36 \pm 0.01) + (0.014 \pm 0.001) \ln s$ (dashed curve).

The difference in the s dependance of ρ^o production for $\pi^* p$ and pp interactions can be qualitatively understood in a simple manner. In either case the contribution to ρ^o production from proton fragmentation is relatively small. Thus the only major source of ρ^o production in pp interactions is expected to be some central mechanism. In $\pi^* p$ interactions, however, ρ^o mesons may also be produced via dissociation of the beam pion, providing a forward component of ρ^o production which is quite important at lower energies but becomes relatively less important as s increases and central production becomes dominant. This effect has been noted before[6, 18], and the beam fragmentation and central production components have been separately estimated in 16 GeV πp interactions. If this simple picture is valid, then one might expect the increase in inclusive ρ^o production to proceed at the same rate in πp and pp interactions for sufficiently large s, if the central production mechanism becomes independent of the nature of the incident particles. Although extrapolation of the fits to presently available data does not lead to such a limit we note that the data of both Fig. 3 and Fig. 4 appear qualitatively consistent with such a picture. The values of both $\sigma(\rho^o)$ and $\langle \rho^o \rangle$ in $\pi^* p$ and pp

interactions may already have converged in the currently available energy range. More precise data on ρ^o production in both $\pi^* p$ and pp interactions are needed for further tests of this hypothesis. Until such data are obtained, cross sections calculated by extrapolation from fits to presently available data must be considered questionable.

C. Characteristics of Semi-Inclusive ρ^o Production

Values of the semi-inclusive ρ^o production cross sections $\sigma_n(\rho^o)$ were presented in Table I for each of our three energies. At a given s the cross sections initially rise with increasing n to a maximum at a value of n which tends to increase with increasing s and then decrease again. The behavior is quite similar to that observed for the semi-inclusive topological inelastic cross sections σ_n. To study this similarity we have listed the values of $\langle \rho^o \rangle_n = \sigma_n(\rho^o)/\sigma_n$ in Table II and have plotted them as a function of n in Fig. 5. The data for all three energies are consistent with approximately the same linear dependence on n. Fits with an expression of the form $\langle \rho^o \rangle_n = an + b$ have been made to the data at each separate s and to the combined data. The results are shown in Table III and Fig. 5. The combined data can be represented (solid line) by the expression $\langle \rho^o \rangle_n = (0.067 \pm 0.003)n - (0.153 \pm 0.033)$ with $\chi^2/DF = 1.17$. Wroblewski[19] has recently published results for fits of $\langle \rho^o \rangle_n$ with the same expression for $\pi^+ p$ and pp interactions as well as $\pi^- p$ interactions. He finds that in all cases a slope of about 0.05 provides a reasonable description, independent of the nature of the incident particles. This again is consistent with the dominance of a central production mechanism.

While the fits are not quantitatively as good, the data may be qualitatively described by an even simpler parametrization, $\langle \rho^o \rangle_n = cn$. The single free parameter c has the values (0.052 ± 0.007), (0.048 ± 0.003) and (0.045 ± 0.003) at 100, 200, and 360 GeV/c, respectively with $\chi^2/DF = 0.55$, 4.15, and 2.57. The fit to the combined data (dashed line) yields $c = 0.047 \pm 0.002$ with $\chi^2/DF = 2.24$.

Since $\langle n \rangle$ rises with $\sqrt{s}$ (in Ref. 2 we quote a fit for π^-p interactions which is $\langle n \rangle = (-1.15 \pm 0.02) + (1.52^{+0.02}_{-0.03}) \sqrt{s}$) either of the fits to $\langle \rho^o \rangle_n$ described above is consistent with a rise in inclusive ρ^o production linear in $\langle n \rangle$ and hence linear in $\sqrt{s}$. Thus the rise in ρ^o cross section is consistent with the same sort of increase observed for the total inelastic cross section.

The expressions for $\langle \rho^o \rangle_n$ described above may be combined with experimental data for σ_n or with parametrizations for σ_n such as the KNO scaling formula[20] to provide predictions of $\sigma_n(\rho^o)$ at other values of s. If we assume

$$\langle n \rangle \frac{\sigma_n}{\sigma_{inel}} = \Psi\left(\frac{n}{\langle n \rangle}\right)$$

where $\Psi\left(\frac{n}{\langle n \rangle}\right)$ is determined from available data for topological cross sections and use the simplest parametrization

$$\langle \rho^o \rangle_n = \sigma_n(\rho^o)/\sigma_n = cn$$

we have

$$\sigma_n(\rho^o) = c\frac{n}{\langle n \rangle} \Psi\left(\frac{n}{\langle n \rangle}\right)$$

$$= \Psi'\left(\frac{n}{\langle n \rangle}\right)$$

We have used our parametrizations of $\langle \rho^o \rangle_n$ to compute values for $\sigma_n(\rho^o)$ in π^-p interactions at other energies where data are available and obtain quite satisfactory agreement with published values.

IV. Comparison of ρ^o Production and Pion Production

It is interesting to compare ρ^o and charged pion production and to estimate the fraction of final-state pions which are daughter products from ρ^o decay. In Fig. 6 we plot data as a function of s for the quantity $\langle \rho^o \rangle / \langle \pi_c \rangle$ where $\langle \pi_c \rangle$ is approximately the number of "non-beam-like" charged pion pairs. The data for both pp and $\pi^\pm p$ interactions are plotted, with $\langle \pi_c \rangle = \langle \pi^- \rangle - 1$ in π^-p interactions and $\langle \pi_c \rangle = \langle \pi^- \rangle$ in pp and π^+p interactions, in Fig. 6. It appears that the data are converging at a value of about 0.12 at large s, suggesting that about 12% of all "produced" charged pions come from the decay of ρ^o mesons. Other estimates of this fraction can be made from our various parametrizations of $\langle \rho^o \rangle_n$ and $\langle \rho^o \rangle$ presented in Section III. The fraction of all final-state charged particles coming from ρ^o decay is just $2\langle \rho^o \rangle / \langle n \rangle$. The variation of $\langle n \rangle$ with s can be used to estimate a high energy limit for this fraction. Our parametrizations of $\langle \rho^o \rangle_n$ lead to estimates that about 10% (9 - 14%) of all charged pions come from ρ^o decay. The parametrizations of $\langle \rho^o \rangle$ and $\sigma(\rho^o)$ based on all the data yield comparable limits at very large s; the parametrizations based on only the high energy π^-p data suggest smaller limits.

In Fig. 7 we compare the production of ρ^o and π^+ mesons in π^-p interactions as a function of p_T^2, the square of the transverse momentum. The values of $d\sigma/dp_T^2$ for ρ^o mesons were determined by fitting $M(\pi^+\pi^-)$ distri-

butions for various intervals of p_T^2 in the manner described in Section II. Again the values obtained for the total ρ^o production cross section by summing the contributions for various p_T^2 intervals are quite consistent with the values quoted in Table I. We observe that above $p_T^2 \approx 0.4$ (GeV/c)^2 the shapes of the ρ^o and π^+ distributions appear quite similar. We have fitted the ρ^o distributions with the simple exponential function $d\sigma/dp_T^2 = Ae^{bp_T^2}$. Results of these fits are given in Table IV. The combined ρ^o data at all three energies yield $d\sigma/dp_T^2(\rho^o)$ (mb/(GeV/c)^2) = $(23.0 \pm 0.8)\exp((-2.57 \pm 0.06)p_T^2)$. The π^+ distribution for 360 GeV/c is shown on the figure; distributions for the other energies are similar. The shape of the π^+ distribution is more complicated but above 0.8 (GeV/c)^2 it can be fitted with a single exponential, $d\sigma/dp_T^2(\pi^+) \propto \exp((-2.48 \pm 0.04)p_T^2)$. We also show in the plot the ratio ρ^o/π^+ as a function of p_T^2. This ratio reaches a value of 0.46 ± 0.14 in the region $1.0 \leq p_T^2 \leq 2.0$ (GeV/c)^2. Our results are quite similar to those obtained at much lower incident energy[4,6]. The ρ^o/π^+ ratio becomes larger as p_T^2 increases.

V. ρ^o Production as a Function of Longitudinal Rapidity

In Fig. 8 we show c.m. rapidity distributions $d\sigma/dy^*$ for ρ^o mesons at each of our three energies. Here $y^* = \frac{1}{2} \ln\left(\frac{E^* + p_L^*}{E^* - p_L^*}\right)$ where E^* and p_L^* are the c.m. energy and longitudinal momentum of the ρ^o meson. The values of the differential cross section $d\sigma/dy^*$ were determined by fitting $M^*(\pi^+\pi^-)$ distributions for various y^* intervals as described in Section II. We also show for comparison the rapidity distributions for inclusive π^+ production in π^-p interactions at 360 and 100 GeV/c and for inclusive π^- production in π^-p interactions at 360 GeV/c. The y^* distributions for ρ^o production appear qualitatively similar to those for π^+ production; there is no clear evidence for a large contribution to ρ^o production from projectile pion fragmentation. The existence of some such contribution cannot be ruled out, however, on the basis of these distributions. It should be noted that the kinematically allowed range of y^* is significantly less for ρ^o mesons than for pions; $|y^*|_{max}$ = 2.89, 3.24, and 3.53 for ρ^o mesons produced at 100, 200, and 360 GeV/c respectively, as compared to $|y^*|_{max}$ = 4.58, 4.93, and 5.23 for pions. There are also experimental difficulties in determining the ρ^o production cross section for fast-forward ρ^o's. The decays can result in very fast pions for which momentum resolution is limited in the 360 GeV/c data even with additional information from the hybrid spectrometer. In determining $d\sigma/dy^*$ for ρ^o production we have attempted to take into account the increased resolution by increasing Γ_o by appropriate amounts in the fits for forward ρ^o production. We have also tried fits using only data from events where hybrid information is available. The resulting values for $d\sigma/dy^*$ from these fits are consistent with those obtained from the whole data sample by increasing Γ_o so we have chosen to plot the latter values for consistency.

In order to study the variation of $d\sigma/dy^*$ with s in various regions of y^* we have obtained fitted values of $\sigma_{\rho^o}(y^*)$ for larger y^* intervals. These values are listed in Table V. First, we have chosen to list values for the intervals $-3.0 < y^* < -1.0$, $-1.0 < y^* < +1.0$, and $+1.0 < y^* < +3.0$ in order to provide comparisons with the work of other experimenters. These intervals

have, however, the disadvantage that they cannot be clearly associated with a particular production mechanism; as s increases, the ρ^0 mesons produced via a "central" mechanism are expected to extend to larger and larger values of $|y^*|$ while the regions populated by ρ^0 mesons from initial particle fragmentation are expected to separate by larger intervals. To avoid this difficulty we have also attempted to define reasonable intervals for fragmentation and central production which vary with s. Unfortunately there is no well-defined criterion by which to separate these regions. We have arbitrarily chosen the fragmentation regions to extend 1.17 units from the maximum y^* allowed for ρ^0 production. This limit corresponds also to approximately the maximum y^* for a ρ^0 with $p_T = 1$ GeV/c and is 2 units less than the maximum y^* for a pion with $p_T = 0.3$ GeV/c. (We are using similar limits in a study of $\pi\pi$ rapidity correlations in the central region.) With regions chosen in this manner, the data of Table V suggest a growing central production cross section, a small and approximately constant ρ^0 production contribution from target proton fragmentation, and a small and apparently decreasing contribution from beam pion fragmentation. A priori one might expect a somewhat larger and more constant contribution from the decay of diffractively produced multipion states in reactions such as $\pi^-p \to X^{*-}p$ followed by $X^{*-} \to \rho^0\pi^-$. We note, however, that such production is expected to be most important for low charge multiplicities. The data in Table I for $\sigma_n(\rho^0)$ seem to indicate a decrease in $\sigma_n(\rho^0)$ at small n as s increases; this would be consistent with our observations above.

If our data for $\sigma(\rho^0)$ in the "central" region are fitted with the form $\sigma_c(\rho^0) = A + B \ln s$, we obtain $\sigma_c(\rho^0)$ (mb) = $(0.09 \pm 0.17) + (1.25 \pm 0.03) \ln s$. This suggests a rise with $\ln s$ in the central production cross section considerably faster than that for the inclusive cross section discussed in Section II. If our choice of a "central" region is reasonable this may indicate that, over the available energy range, the variation in $\sigma(\rho^0)$ is determined by a rise in central ρ^0 production combined with a decrease in ρ^0 production from initial particle fragmentation. If this is the case we may expect to see a somewhat more rapid rise in $\sigma(\rho^0)$ at larger s that that predicted by our fit in Section II. The variation in the ρ^0 cross section for $-1.0 < y^* < +1$ has been fitted as $\sigma_0(\rho^0)$ (mb) = $(-2.2 \pm 3.6) + (1.09 \pm 0.58) \ln s$. It appears that, in addition to the widening of the plateau expected for ρ^0 production, the differential cross section near $y^* = 0$ may still be increasing.

VI. Summary

We have studied ρ^0 production in π^-p interactions as a function of s and n, using our own data at 100, 200, and 360 GeV/c together with other published data. We find that both the inclusive $\sigma(\rho^0)$ and $\langle \rho^0 \rangle$ are consistent with an s dependence of the form $\sigma(\rho^0) = A + B \ln s$. Values of $\langle \rho^0 \rangle / \langle \pi_c \rangle$ in both π^+p and pp interactions seem to approach the same constant value of ~ 0.12. All of our data on $\langle \rho^0 \rangle_n = \sigma_n(\rho^0)/\sigma_n$ as a function of n are consistent with the form $\langle \rho^0 \rangle_n = an + b$. This regularity coupled with values for the σ_n may be used to estimate semi-inclusive ρ^0 cross sections at other energies.

The y^* and p_T^2 dependence of ρ^0 production seem qualitatively similar to that of produced pions having charge different from that of the beam pion. At

large p_T^2 values ($1.0 < p_T^2 < 2.0$ (GeV/c)^2) the ratio of ρ^o/π^+ is approximately 0.5.

The observed ρ^o production at these energies appears to be primarily due to a central production mechanism. Details of the s dependence of the ρ^o cross section for various regions of y^* have been presented.

Acknowledgments

We wish to thank the Fermilab staff and the crew of the 30-inch bubble chamber for their aid in performing these experiments. Special thanks are due to our analysis and technical staffs. This work was supported in part by the National Science Foundation, the U. S. Department of Energy, and the National Research Council of Canada.

Appendix A. Effective-Mass Background Distributions Using Tracks from Different Events.

Jancso et al.[9] have determined cross sections for neutral vector meson production in pp interactions at $\sqrt{s}$ = 53 GeV by a method which involves construction of background distributions from pairs of tracks randomly selected from different events. The resulting $M(\pi^*\pi^*)$ distributions are normalized to their experimental distributions in the mass region 2 GeV < $M(\pi\pi)$ < 4 GeV where resonance production is not expected to play a significant role. They find that the background provides an excellent description of their $(\pi^+\pi^+ + \pi^-\pi^-)$ mass distribution. The excess above the background observed in the $M(\pi^+\pi^-)$ distribution is then fitted with a sum of contributions from ω^o, ρ^o, K^{*o} (with the K-meson treated as a pion), and f^o decay. The resulting estimates for ρ^o production are considerably larger than estimates obtained at lower energies by more conventional methods. We have tried similar methods of background construction in fitting our data and have not obtained acceptable results.

Our data differ from those of Jancso et al. in that we have events of exactly known charge multiplicity with momentum determinations for all charged tracks. The data from the Split Field Magnet detector at the ISR consisted typically of events in which some tracks could not be observed or reconstructed. Exact charge multiplicities were generally not known and tracks with c. m. momenta < 0.3 GeV/c or $\Delta p/p > 0.30$ were not used in their analysis. Background distributions constructed by combining randomly selected tracks from different events are expected to take into account detector acceptance and combinatorial problems. However, such backgrounds do not include exactly the effects of momentum and energy conservation.

We have constructed background dipion effective mass distributions both by selecting pairs of tracks from different events of all multiplicities and by selecting pairs of tracks only from events of the same charge multiplicity. The latter method might be expected to better approximate the constraints of momentum and energy conservation. It also allows the construction of background distributions for the semi-inclusive $M(\pi\pi)$ distributions. The background estimates have been normalized to the data in the mass region 2.0 GeV < $M(\pi\pi)$ < 4.0 GeV.

The backgrounds constructed for the $(\pi^+\pi^+ + \pi^-\pi^-)$ mass distributions did not provide a good description of the data in the mass region below 2 GeV. When pairs of tracks randomly selected from events of all multiplicities are used, the background curve falls below the data everywhere in the region $M(\pi\pi)$ < 2.6 GeV. When pairs are selected only from events with the same charge multiplicity the background exceeds the data over most of the region $M(\pi\pi)$ < 2.0 GeV as shown in Fig. 9a for 369 GeV/c data. For $M(\pi\pi)$ < 0.4 GeV a sharp peak is observed in the difference between data and background. We attribute this peak to second-order interference effects (Bose-Einstein effects) for pions of like charge[21]. When backgrounds for fixed charge multiplicity are compared with the data similar results are obtained. The background exceeds the data for $M(\pi\pi)$ < 2.0 GeV/c except near threshold, where sharp peaks are observed for $n \geq 8$. Thus the study of backgrounds for like-charge pairs indicates that this method does not provide an adequate description of the data.

Backgrounds have also been constructed for the $M(\pi^+\pi^-)$ distributions in a similar manner. The difference between the inclusive $M(\pi^+\pi^-)$ distribution at 360 GeV/c and the background constructed from pairs drawn from events of the same multiplicity is shown in Fig. 9b. The background falls below the data for $M(\pi^+\pi^-) \leq 1$ GeV and a peak can be seen at the ρ^0 mass. If all of the excess in the region $0.60 < M(\pi^+\pi^-) < 0.92$ GeV is attributed to ρ^0 production, the corresponding cross section is about 9 mb. At 200 GeV/c the excess is about 5.5 mb. However, a study of $M(\pi^+\pi^-)$ distributions for fixed charge multiplicity provides further evidence against the validity of this method for estimating background. At 360 GeV/c the background estimates are below the data at all n. However, at 200 GeV/c the background estimates lie above the data in the resonance region for all $n \geq 14$. Use of background constructed from pion pairs selected from different events of all multiplicities yields much larger estimates for ρ^0 production cross sections; at 200 GeV/c there is an excess of about 16 mb in the ρ^0 region. However, if we assume that the background is underestimated by an amount equal to the difference observed in the $(\pi^+\pi^+ + \pi^-\pi^-)$ distribution, the remaining excess would be only about 3 mb.

We conclude that the technique of constructing background mass distributions from tracks drawn from different events does not provide a reliable method for estimating production cross sections for vector meson resonances. Good representations of mass distributions for pairs of pions of the same charge cannot be obtained and the method clearly fails for $\pi^+\pi^-$ distributions at fixed charge multiplicity.

References

(a) Present address: Argonne National Laboratory, Argonne, Illinois 60439
(b) Present address: Department of Physics, Case Western Reserve University, Cleveland, Ohio 44106
(c) Present address: Department of Physics, University of Toronto, Toronto, Ontario M5S 1A7, Canada

1. N.N. Biswas et al., Phys. Rev. Lett. 35, 1059 (1975); G.A. Smith, in Particles and Fields - 1973, Proceedings of the Berkeley Meeting of the Division of Particles and Fields of the APS, edited by H. Bingham et al., (AIP, New York, 1974); E.D. Fokitis, Ph.D. Dissertation, University of Notre Dame, 1976 (unpublished); F.C. Svrcek, University of Maryland Technical Report No. 77-039, PP. No. 77-134, November (1976).

2. E.L. Berger et al., Nucl. Phys. B77, 365 (1974); 100 GeV/c.
D. Ljung et al., Phys. Rev. D15, 3163 (1977); 200 GeV/c.
A. Firestone et al., Phys. Rev. D14, 2902 (1976); 360 GeV/c.

3. V.V. Anisovitch and V.M. Shekter, Nucl. Phys. 55B, 455 (1973); Nucl. Phys. 63B, 542 (1973).

4. M. Deutschmann et al., Nucl. Phys. B103, 426 (1976); 8, 16, 23 GeV/c π^+p.

5. J. Brau et al., Nucl. Phys. B99, 232 (1975); 15 GeV/c π^-p.

6. J. Bartke et al., Nucl. Phys. B107, 93 (1976); 16 GeV/c π^-p.

7. Particle Data Group, Rev. Mod. Phys. 48, S1 (1976).

8. P.D. Higgins, Ph.D. Dissertation, University of Notre Dame, 1978 (unpublished).

9. G. Jancso et al., Nucl. Phys. B124, 1 (1977).

10. D. Fong et al., Phys. Lett. 60B, 124 (1975); 147 GeV/c π^-p.

11. R. Singer et al., Phys. Lett. 60B, 385 (1976); 205 GeV/c pp.

12. P. Berzatta et al., Nuovo Cimento 15A, 45 (1973); 11.2 GeV/c π^-p.

13. H.A. Gordon et al., Phys. Rev. Lett. 34B, 284 (1975); 22 GeV/c π^+p.

14. V. Blobel et al., Phys. Lett. 48B, 73 (1974); 12, 24 GeV/c pp.

15. V. Ammosov et al., Proceedings of the Palermo Conference (1975); 69 GeV/c π^-p.

16. N. Angelov et al., Yad.Fiz. 25, 117 (1977); 40 GeV/c π^-p.

17. In a previous study of ρ^0 production for the 205 GeV/c π^-p reaction, F.C. Winkelmann et al., Phys. Lett. 56B, 101 (1975), the ρ^0 production cross section was reported to be 13.5 ± 3.4 mb. As this result was based on a subsample of the current data, we do not include this in Fig. 3 and other relevant figures.

18. P.V. Chliapnikov, Plenary Report on Multiparticle and Inclusive Reactions, submitted to the 18th International Conference on High Energy Physics, Tbilisi (1976).

19. A. Wroblewski, Proceedings of the VIII International Symposium on Multiparticle Dynamics (Kaysersberg), A-1 (1977).

20. Z. Koba, H.B. Nielsen, P. Olesen, Nucl. Phys. B40, 317 (1972).

21. N.N. Biswas et al., Phys. Rev. Lett. 37, 175 (1976).

Table I

Semi-Inclusive and Inclusive ρ^0 Production Cross Sections[a] (in mb)

n	p_{lab} (GeV/c) 100	200	360
4	0.77 ± 0.16	0.47 ± 0.11	0.25 ± 0.05
6	1.54 ± 0.25	0.88 ± 0.18	0.74 ± 0.13
8	2.11 ± 0.46	2.12 ± 0.27	1.14 ± 0.23
10	1.16 ± 0.50	1.82 ± 0.25	1.87 ± 0.19
12	1.23 ± 0.45	1.89 ± 0.20	1.57 ± 0.15
14	0.83 ± 0.43	1.12 ± 0.20	1.08 ± 0.15
(≥)16	0.22 ± 0.20	0.29 ± 0.27	1.03 ± 0.23
(>)18		0.18 ± 0.18	0.36 ± 0.12
20			0.24 ± 0.05
(≥)22			0.0 ± 0.10
Inclusive			
A. (Sum)	7.86 ± 0.99	8.77 ± 0.63	8.28 ± 0.48
B. (Inclusive fit)	7.49 ± 1.79	8.36 ± 0.80	8.49 ± 0.29
C. (Sum of y^*-region fits)	7.60 ± 0.55	8.40 ± 0.72	8.65 ± 0.23
D. Weighted average of A, B, C)[b]	7.65 ± 0.46	8.54 ± 0.41	8.55 ± 0.17

[a] Errors include some allowance for uncertainties in the fit parametrization.
[b] In computing D, determinations A, B, and C have been treated as independent. The quoted errors on the weighted average do not include any additional contribution for systematic uncertainties.

Table II

$\langle \rho^0 \rangle = \sigma_n(\rho^0)/\sigma_n$

n	p_{lab} (GeV/c) 100	200	360
4	0.16 ± .05	0.13 ± .03	0.08 ± .03
6	0.30 ± .08	0.22 ± .05	0.21 ± .05
8	0.49 ± .11	0.51 ± .07	0.29 ± .06
10	0.46 ± .20	0.55 ± .08	0.54 ± .06
12	0.87 ± .32	0.86 ± .10	0.61 ± .06
14	1.32 ± .73	1.00 ± .19	0.66 ± .09
16	--	0.47 ± .44	1.06 ± .24
18	--	--	0.70 ± .24
20	--	--	1.13 ± .26

Table III

Fit Parameters in $\langle \rho^o \rangle_n = an + b$

	P_{lab} (GeV/c)			
Parameter	100	200	360	Combined
a	0.076 ± 0.006	0.082 ± 0.010	0.064 ± 0.003	0.067 ± 0.033
b	-0.146 ± 0.034	-0.222 ± 0.054	-0.175 ± 0.020	-0.153 ± 0.033
χ^2/DF	0.27	1.60	0.69	1.17

Table IV

Fit Parameters in $d\sigma/dp_T^2 = Ae^{bp_T^2}$

	P_{lab} (GeV/c)			
Parameter	100	200	360	Combined
A	20.8 ± 3.4	26.7 ± 3.5	22.5 ± 2.1	23.0 ± 0.8
b	-2.48 ± 0.11	-3.05 ± 0.33	-2.49 ± 0.17	-2.57 ± .06

Table V

ρ^o Cross Section in mb as a Function of y^*

	P_{lab} (GeV/c)		
y^* Region	100	200	360
$-3 < y^* < -1$	0.49 ± 0.19	2.11 ± 0.24	2.68 ± 0.22
$-1 < y^* < +1$	3.76 ± 0.90	4.16 ± 0.40	4.93 ± 0.25
$+1 < y^* < +3$	2.83 ± 0.55	2.20 ± 0.40	1.16 ± 0.25
backward[a]	0.28 ± 0.14	0.17 ± 0.08	0.28 ± 0.23
central[b]	6.56 ± 0.51	7.96 ± 0.71	8.24 ± 0.22
forward[c]	0.76 ± 0.10	0.27 ± 0.06	0.13 ± 0.07

[a] $y^* < -1.72$, -2.07, and -2.36 at 100, 200 and 360 GeV/c.

[b] $|y^*| < 1.72$, 2.07, and 2.36 at 100, 200 and 360 GeV/c.

[c] $y^* > +1.72$, +2.07, and +2.36 at 100, 200 and 360 GeV/c.

Figure Captions

Fig. 1 Inclusive $\pi^+\pi^-$ mass distributions for the process $\pi^-p \to (\pi^+\pi^-)X^0$ at (a) 100, (b) 200, and (c) 360 GeV/c. The solid curves represent fits to the data as described in the text. The dashed curves indicate the background contributions.

Fig. 2 Semi-inclusive $\pi^+\pi^-$ mass distributions for (a) n = 6, (b) n = 8, (c) n = 10, and (d) n = 12 in 100, 200, and 360 GeV/c π^-p interactions. The solid curves represent fits described in the text. The dashed curves indicate the background contributions.

Fig. 3 Inclusive ρ^0 production cross sections as a function of s for π^+p and pp interactions. The solid lines represent the fits to all the data described in the text. The dashed line represents the fit to the π^-p data above $s = 100$ GeV^2.

Fig. 4 The average number of ρ^0 mesons per inelastic event, $\langle \rho^0 \rangle$, plotted as a function of s for $\pi^\pm p$ and pp interactions. The solid lines represent the fits to all the data described in the text. The dashed line represents the fit to the π^-p data above $s = 100$ GeV^2.

Fig. 5 Values of $\langle \rho^0 \rangle_n = \sigma_n(\rho^0)/\sigma_n$ as a function of charge multiplicity n for 100 (o), 200 (a), and 360 (x) GeV/c π^-p interactions. The lines represent fits described in the text.

Fig. 6 The ratio $\langle \rho^0 \rangle / \langle n_c \rangle$ (see text) as a function of s for π^+p and pp interactions.

Fig. 7 Distributions of $d\sigma/dp_T^2$ for ρ^0 mesons in 100, 200, and 360 GeV/c π^-p interactions and for π^+ mesons in 360 GeV/c π^-p interactions. The lines represent fits described in the text.

Fig. 8 The c.m. rapidity distributions $d\sigma/dy^*$ for ρ^0 mesons at 100 (o), 200 (a), and 360 (x) GeV/c. Also shown for comparison are $d\sigma/dy^*(x\ 0.1)$ for $\pi^-p \to \pi^+X^-$ at 100 and 360 GeV/c and for $\pi^-p \to \pi^-X^+$ at 360 GeV/c.

Fig. 9 Distributions of the difference between experimental distributions of $M(\pi\pi)$ and background distributions of pion pairs constructed from pions selected from different events of the same charge multiplicity in 360 GeV/c π^-p interactions. The background distributions are normalized to the data in the mass region $2.0 < M(\pi\pi) < 4.0$ GeV. Difference distributions are shown for pion pairs of like and unlike charge.

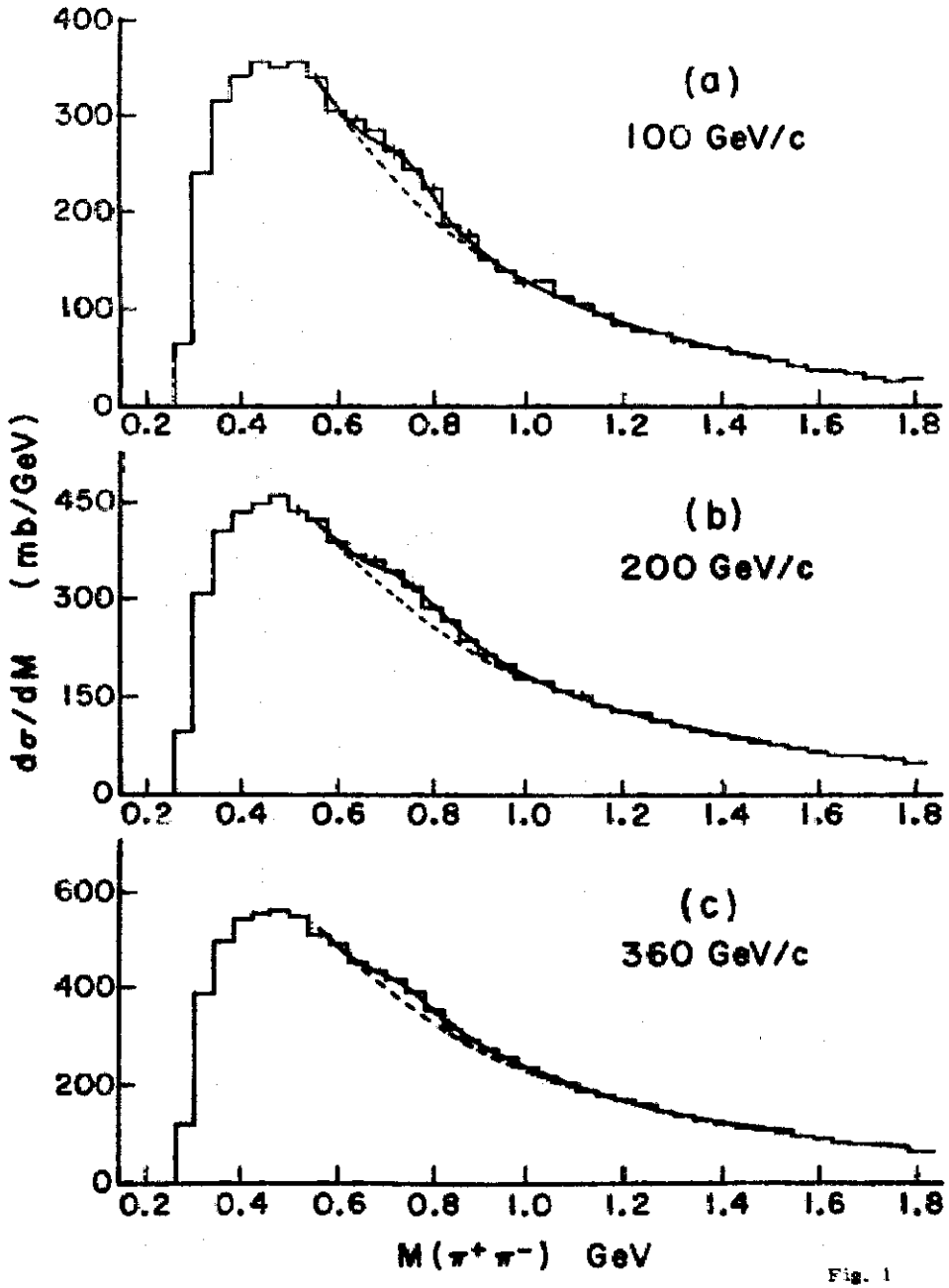
(a)
100 GeV/c
(b)
200 GeV/c
(c)
360 GeV/c
dσ/dM (mb/GeV)
M(π⁺π⁻) GeV

Fig. 1

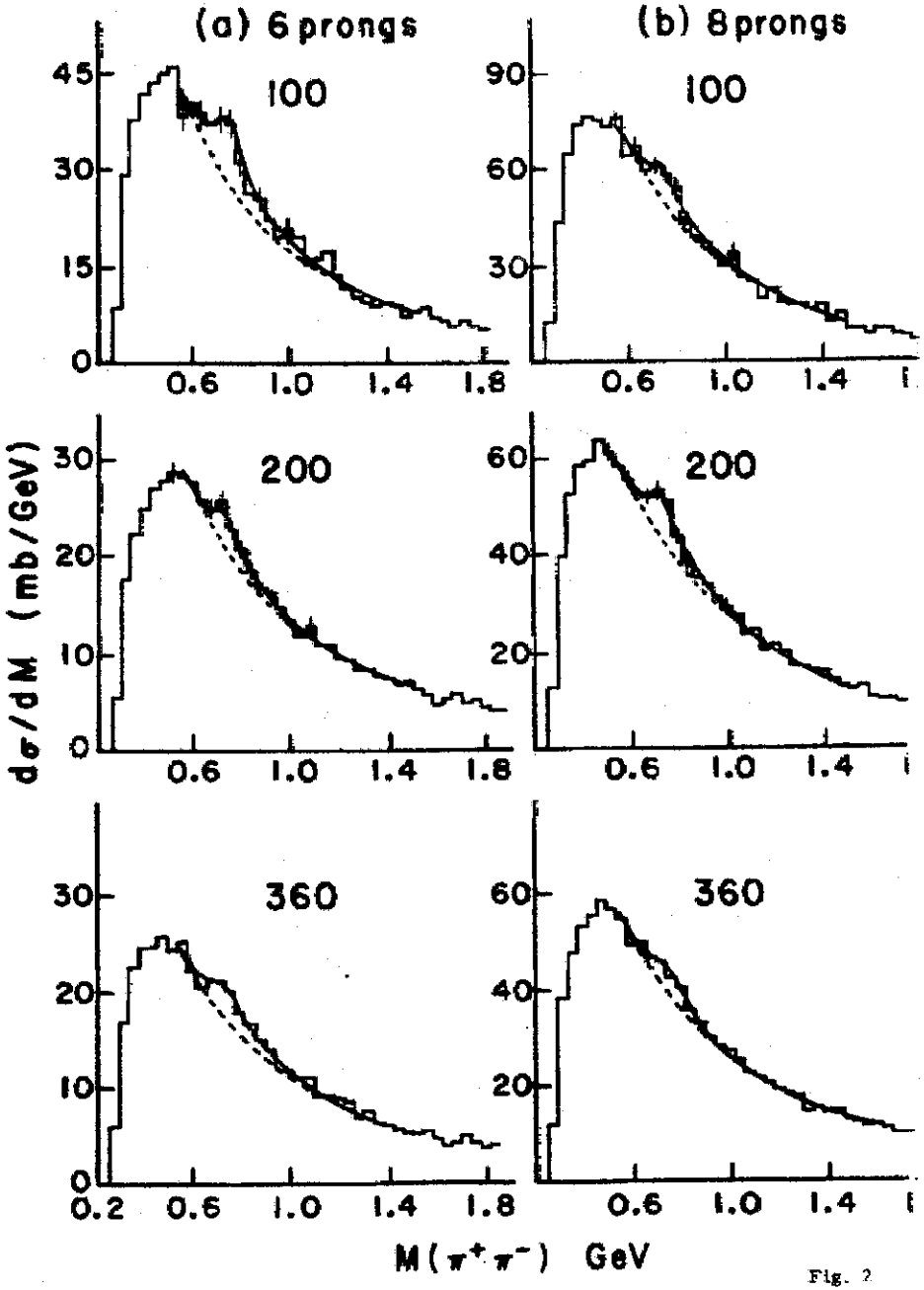
(a) 6 prongs
(b) 8 prongs
100
200
360
dσ/dM (mb/GeV)
M(π⁺π⁻) GeV

Fig. 2

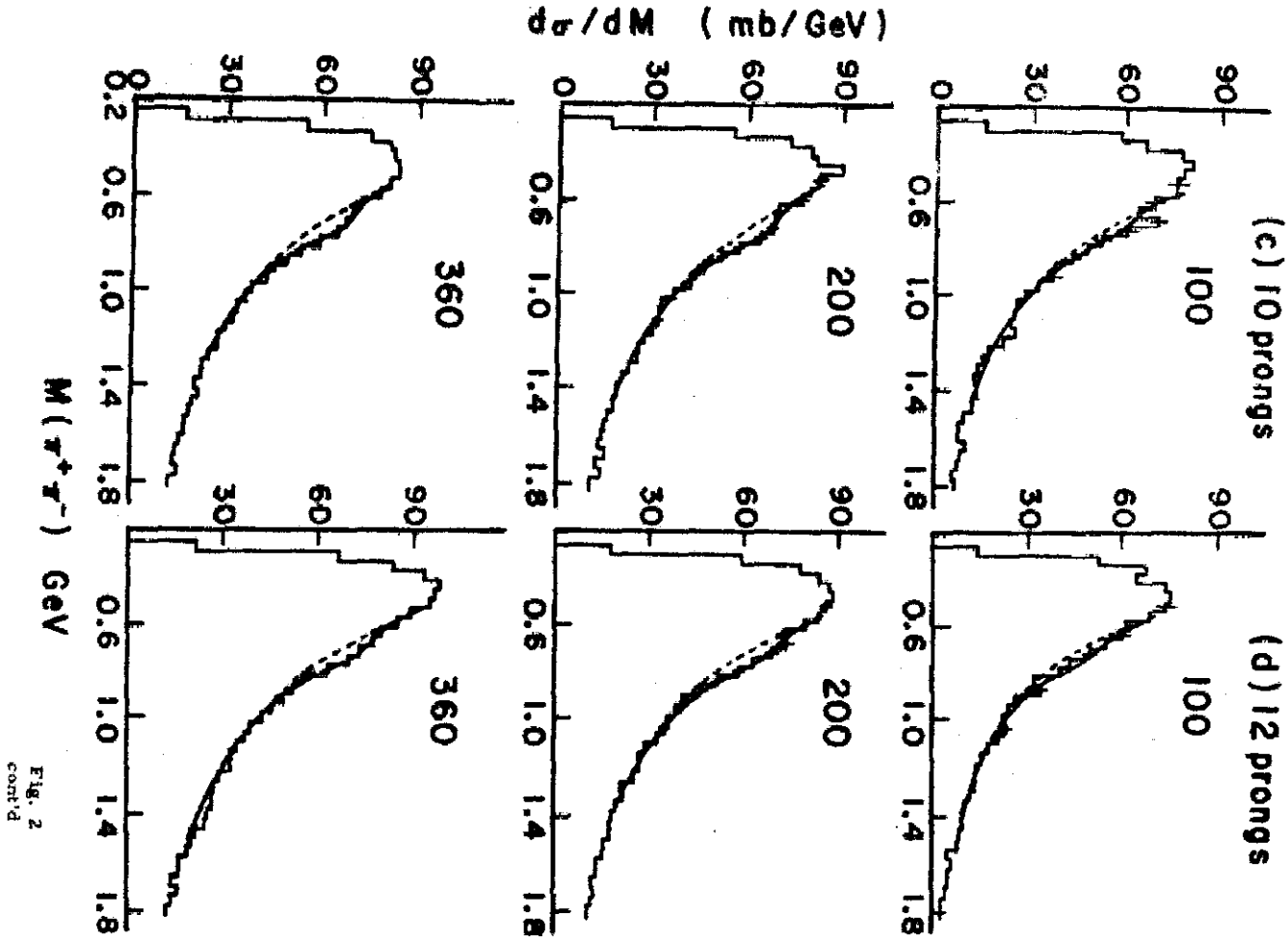

Fig. 2 cont'd

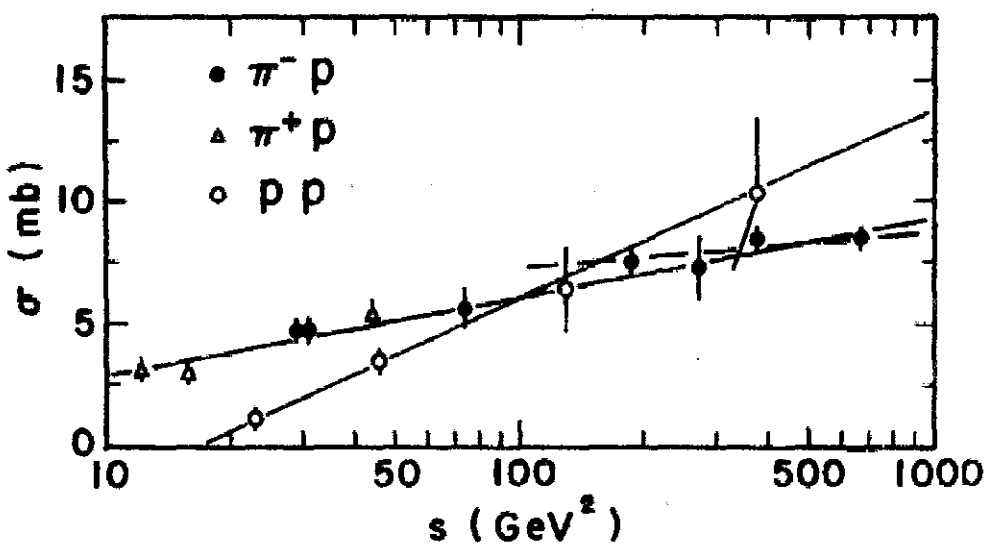

Fig. 3

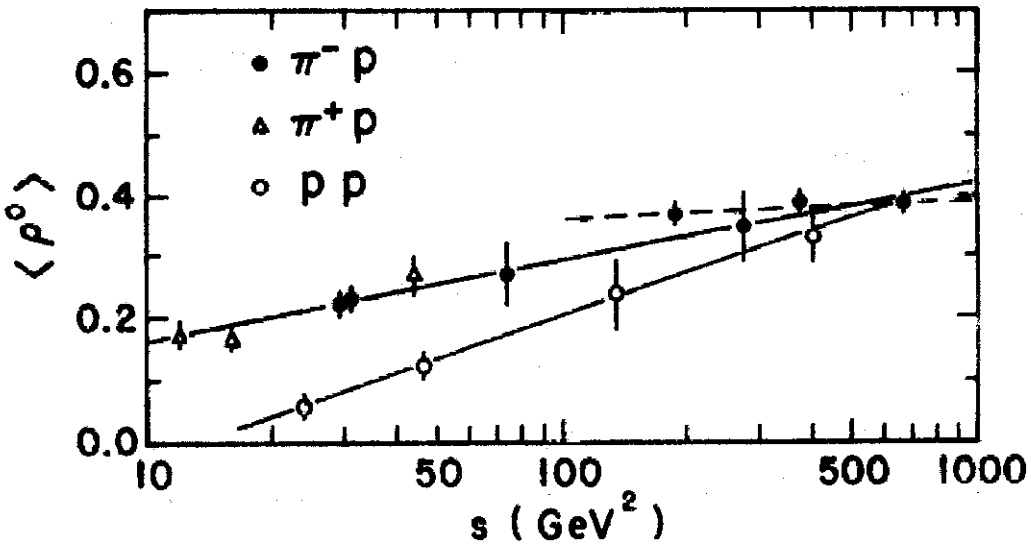
0.6
0.4
0.2
0.0
$\langle \rho^0 \rangle$
$\pi^- p$
$\pi^+ p$
$p p$
10
50
100
500
1000
s (GeV^2)

Fig. 4

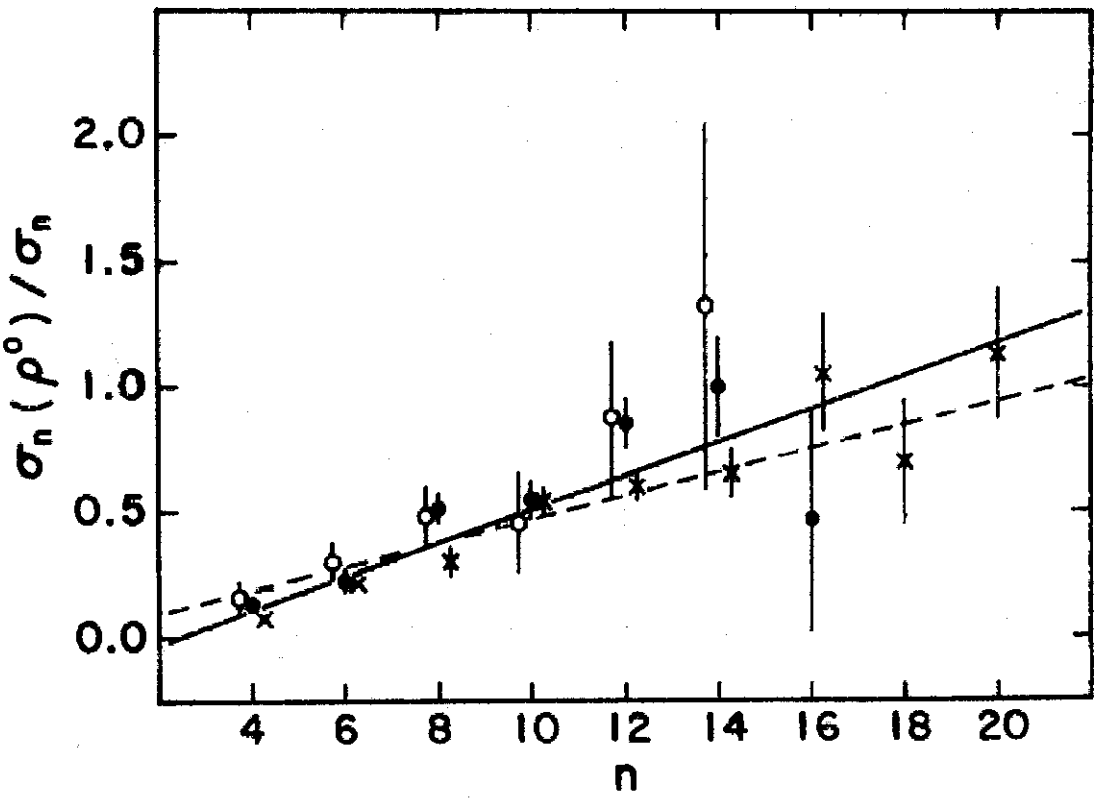
2.0
1.5
1.0
0.5
0.0
$\sigma_n (\rho^0) / \sigma_n$
4
6
8
10
12
14
16
18
20
n

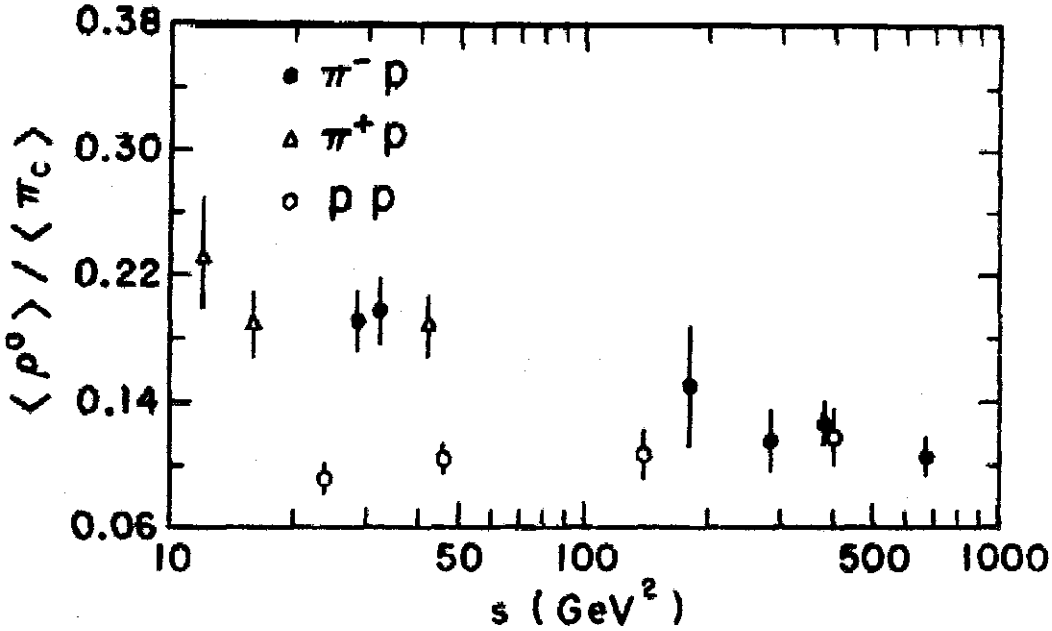
0.38
0.30
0.22
0.14
0.06
10
50
100
500
1000
$\pi^- p$
$\pi^+ p$
$p\,p$
$\langle \rho^0 \rangle / \langle \pi_c \rangle$
$s\ (GeV^2)$

Fig. 6

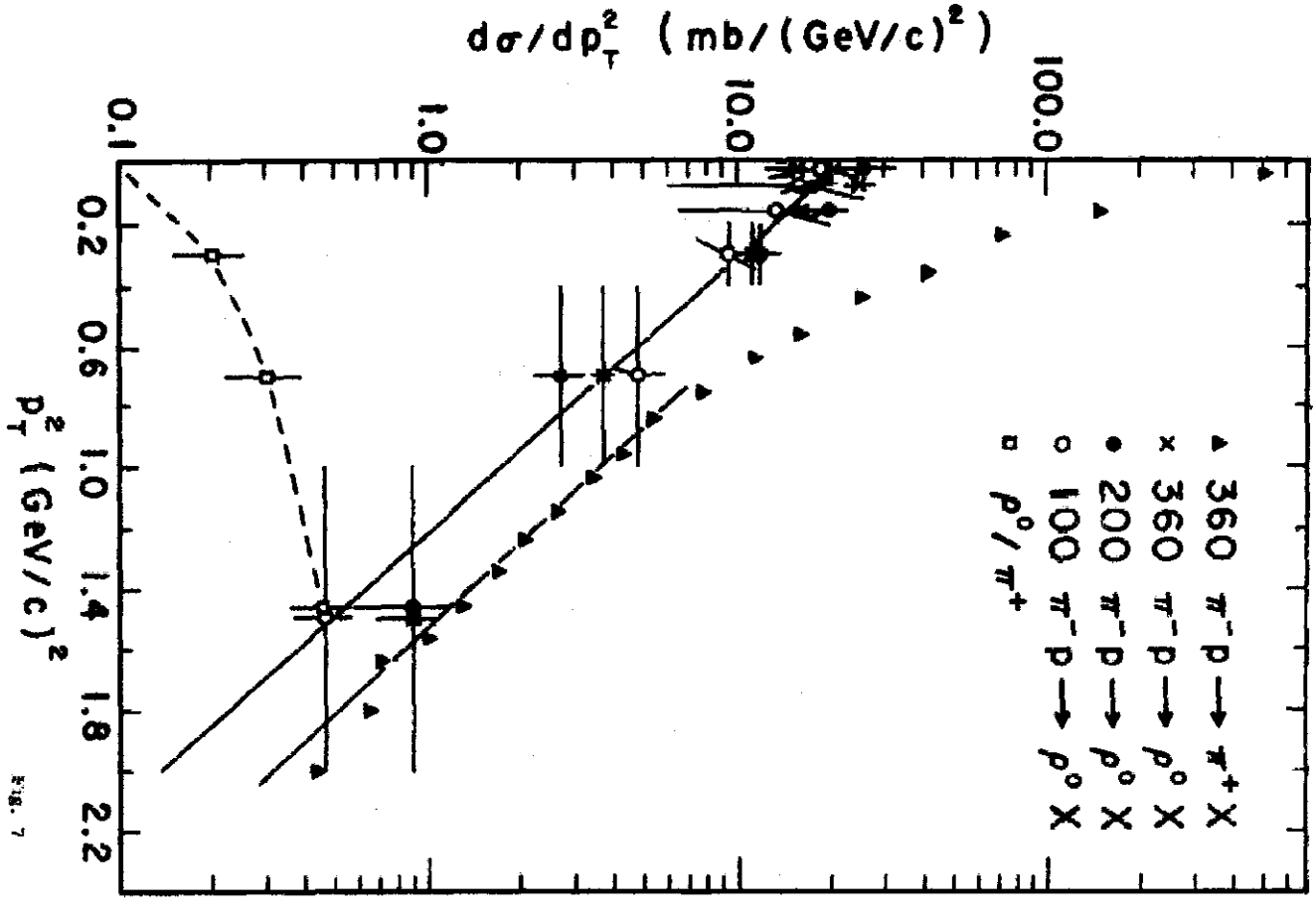
$d\sigma/dp_T^2$ (mb/(GeV/c)^2)
0.1
1.0
10.0
100.0
0.2
0.6
1.0
1.4
1.8
2.2
p_T^2 (GeV/c)^2
$\pi^- p \to \pi^+ X$
$\pi^- p \to \rho^0 X$
$\pi^- p \to \rho^0 X$
$p\,p \to \rho^0 X$
360
360
200
100
ρ^0/π^+

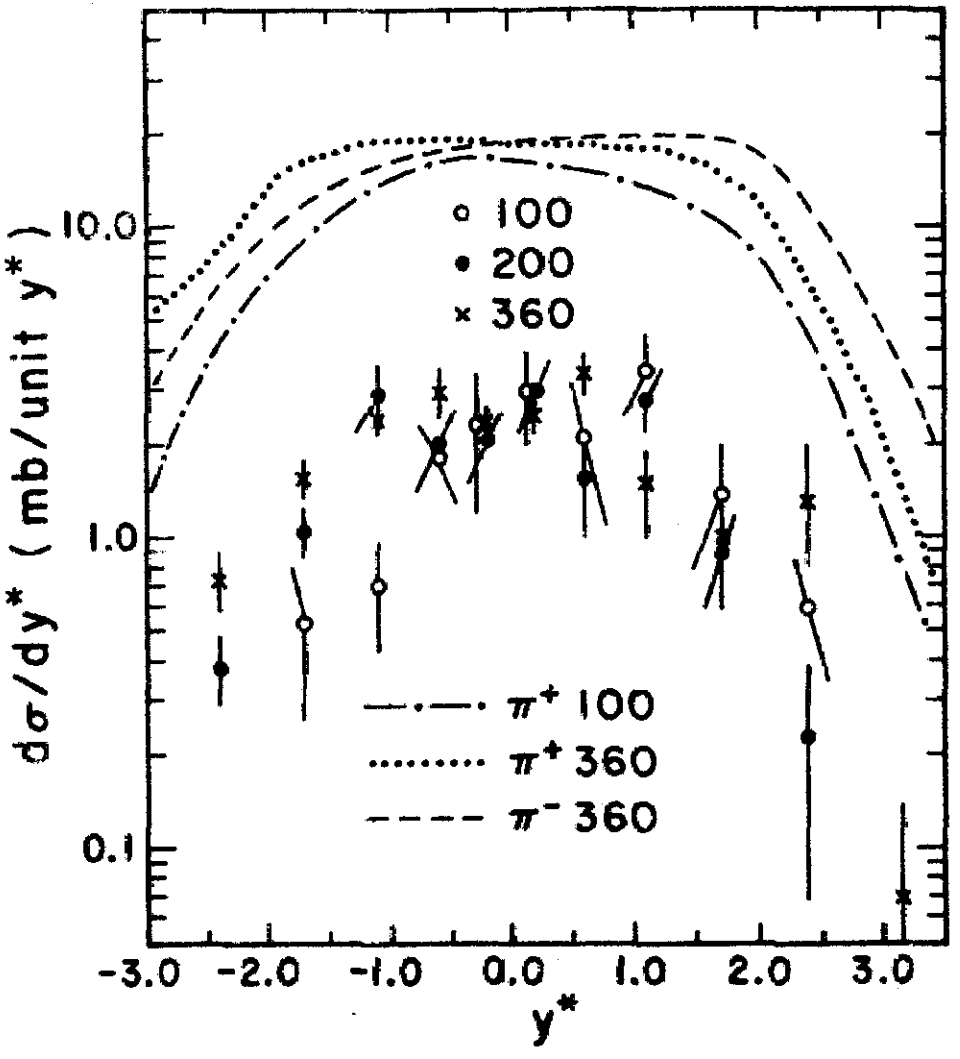
dσ/dy* (mb/unit y*)
10.0
1.0
0.1
o 100
• 200
× 360
π⁺ 100
π⁺ 360
π⁻ 360
-3.0
-2.0
-1.0
0.0
1.0
2.0
3.0
y*

Fig. 8

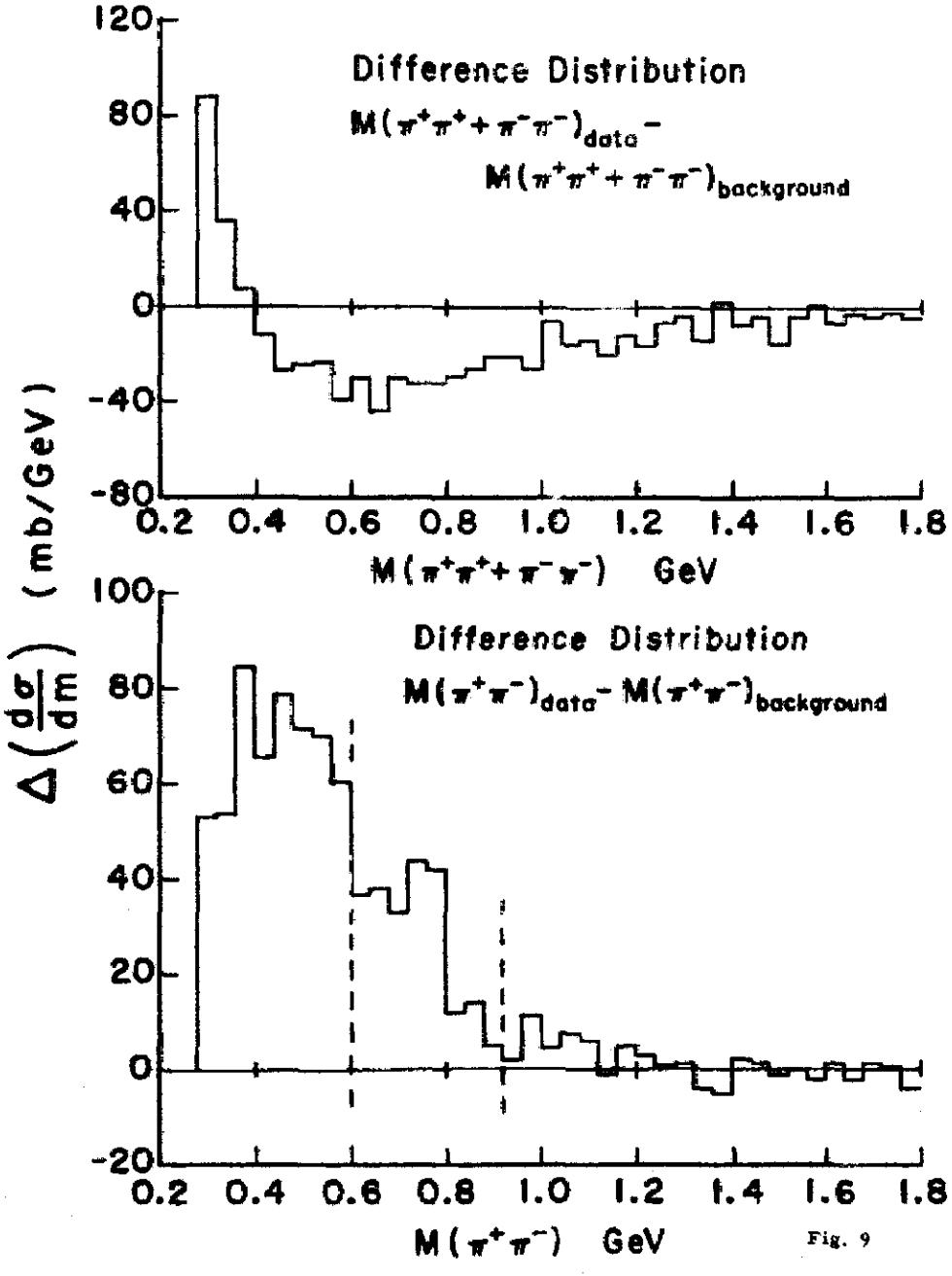
Difference Distribution
M(π⁺π⁺ + π⁻π⁻)data -
M(π⁺π⁺ + π⁻π⁻)background
120
80
40
0
-40
-80
0.2
0.4
0.6
0.8
1.0
1.2
1.4
1.6
1.8
M(π⁺π⁺ + π⁻π⁻) GeV
Difference Distribution
M(π⁺π⁻)data - M(π⁺π⁻)background
Δ(dσ/dm) (mb/GeV)
100
80
60
40
20
0
-20
M(π⁺π⁻) GeV

Fig. 9